Inversion and attribute-assisted hydraulically-induced microseismic fracture prediction: A North Texas Barnett Shale case study

*Xavier E. Refunjol *, Katie M. Keranen, and Kurt J. Marfurt, The University of Oklahoma*

Summary

The goal of this project is to predict possible zones of fracture network propagation during hydraulic stimulation by analyzing seismic attributes and acoustic impedance inversion volumes in the North Texas Barnett Shale. Both volumetric curvature attributes and acoustic impedance inversion volumes demonstrate correlation with hydraulically fractured zones. The characteristics of the rocks within which the microseismic events cluster serve as characterization and prediction tools for determining weakness planes and fracture-prone zones from 3D surface seismic acquired before hydraulic stimulation. The ultimate objective is to minimize the number of wells and thereby cost necessary to fully produce the resource by having *a priori* knowledge of most likely fracture propagation trends and where the formations will most likely fail.

Introduction

The Fort Worth Basin deepens towards the north and its axis roughly parallels the Muenster Arch with a NW-SE trend. The basin is bound to the north by Red River and Muenster arch basement uplifts. The Mineral Wells Fault crosses the northeastern portion of the basin with a NE-SW trend, similar to the southeastern bounding Ouachita Thrust Fault. For this investigation we used a pre-stack time migrated seismic survey from North Texas acquired prior to the hydraulic stimulation. Four vertical wells with P and S-wave logs served as monitor wells for four corresponding horizontal Barnett Shale stimulation wells. The formations were hydraulically fractured in several intervals (or stages) in the horizontal part of the well.

Hydraulically induced fracture network from borehole-based microseismic monitoring

Now a standard procedure in gas shale formations, hydraulic fracture stimulation is used to increase permeability and reactivate natural fractures, as studied by Williams-Stroud and Duncan (2008), and Eiser et al. (2010). During stimulation, energy released by rock failure is recorded by a down-hole array of geophones in a nearby monitor well. Careful processing of the data allows us to locate the fracture network. These induced fractures preferably align with the maximum horizontal stress direction, such that stimulation wells are commonly drilled perpendicular to the maximum horizontal stress to maximize propagation (Neale, 2010). There is a possibility that wells drilled perpendicular to the maximum horizontal stress direction are less stable during both drilling and production stages (Zhang et al., 2006).

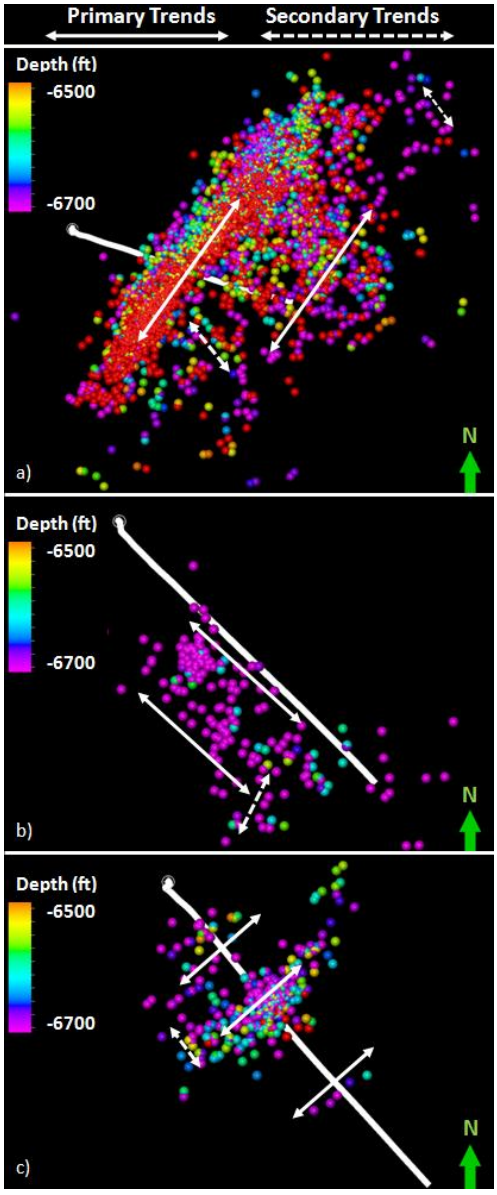

Figure 1. Microseismic event clouds in horizontal portion of wells within the Barnett Shale with a) NE-SW trend following the Mineral Wells Fault, b) NW-SE orientation that parallels the Muenster Arch, and c) a NE-SW trend.

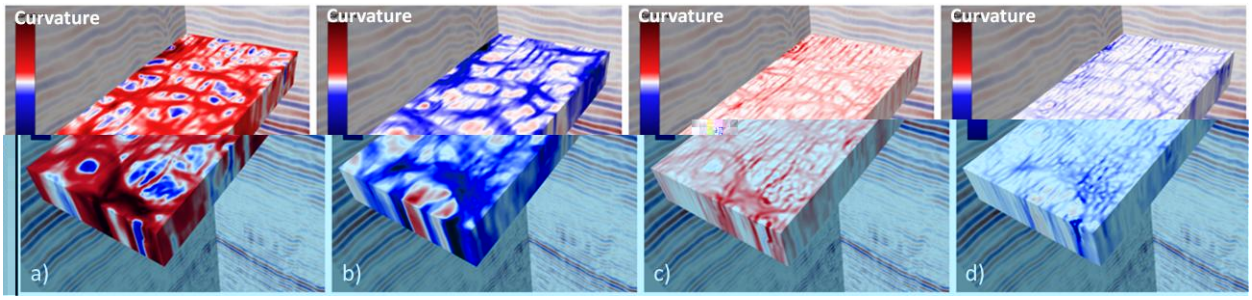

Figure 2. Strat-cubes through a) long-wavelength most-positive curvature, b) long-wavelength most-negative curvature, c) short-wavelength most-positive curvature, and d) short-wavelength most-negative curvature. Note the strong acquisition footprint on the short-wavelength curvature volumes.

In this dataset microseisms highlight features that demonstrate both the influence of the current stress regime and regional tectonic features. Figure 1a shows microseismic events that exhibit a NE-SW preferential orientation, mimicking the major Mineral Wells, the Ouachita Thrust Faults and the presumed current horizontal maximum stress (Gale et al., 2007). In contrast, Figure 1b shows microseismic events that exhibit a nearly perpendicular NW-SE orientation, parallel to another major structure, the Muenster Arch. Figure 1c exhibits trends similar to the ones in Figure 1a and secondary perpendicular lineaments. Since induced fractures preferably occur initially along maximum horizontal stress direction but can be influenced or captured by existing structures, it is possible that a secondary direction may develop that differs from the current stress regime. We will explore the temporal patterns of microseismic activity in our dataset to better understand the multiple orientations of microseismicity.

Volumetric Curvature Attribute

Volumetric curvature attributes have successfully imaged a wide array of features that highlight both the influence of the current stress regime and regional tectonic features. By using long wavelength curvature as well as short wavelength curvature we can observe the different aspects of the same geology. As discussed in Chopra and Marfurt (2007), short wavelength curvature delineates details within intense, highly localized fracture systems. Conversely, long wavelength curvature often enhances subtle flexures correlative to fracture zones below seismic resolution and collapse features that result in broader depressions.

In this case long wavelength most positive and most negative curvature show features that mimic the Mineral Wells and Ouachita Thrust Faults (Figures 2a and b). Short wavelength curvature, while also displaying a strong influence of the regional features, shows smaller secondary features that differ from the current stress regime (Figures 2c and d).

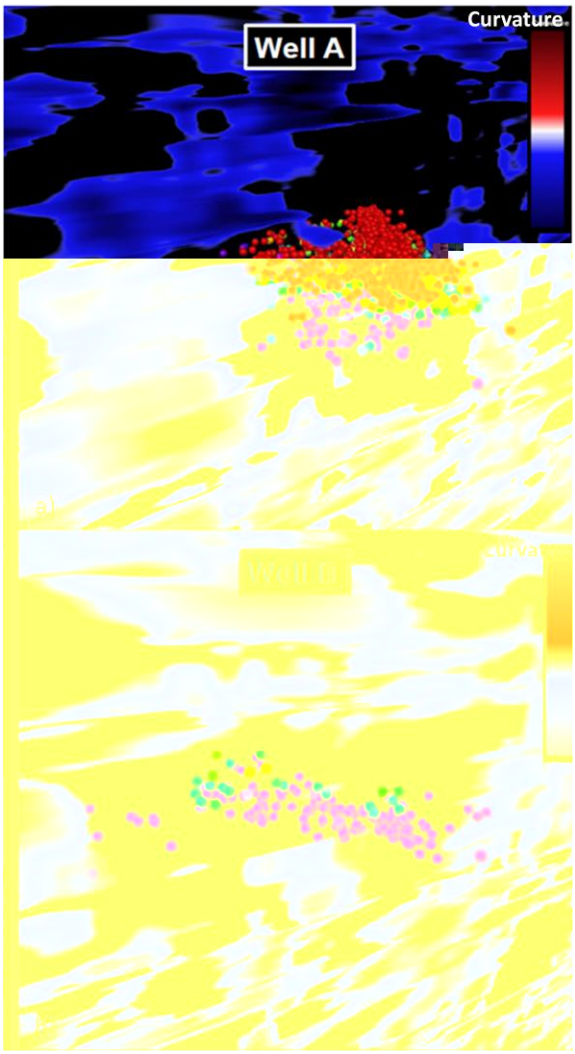

Figure 3. Long wavelength most negative curvature vertical cross sections through microseismic event clouds in a) well A and b) well B.

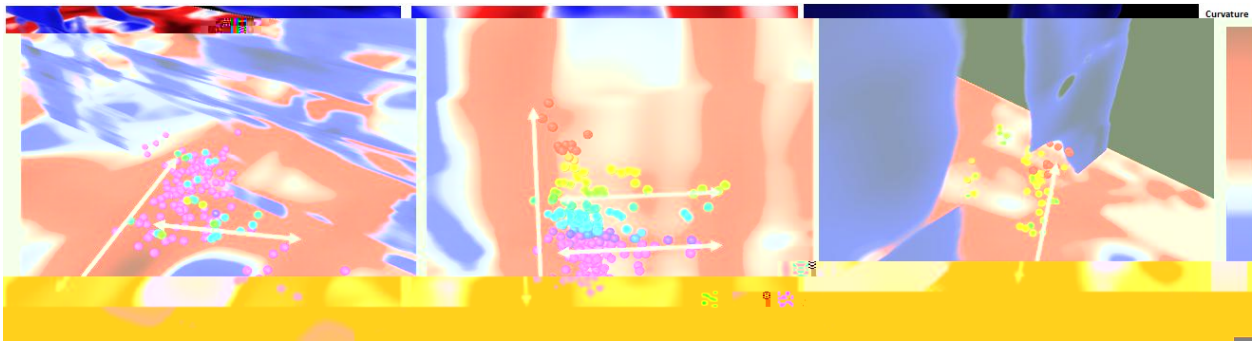

Figure 4. Long wavelength most negative curvature vertical cross sections with most positive curvature time slices through microseismic event clouds in a) well A, b) well B, and well C.

The volumetric curvature attributes show an evident relationship to the microseisms. In the most negative curvature volume, events occur away from the most negative values (Figure 3), favoring areas with high positive curvature in the most positive curvature volume (Figure 4), as hinted by studies of Mai et al. (2009). For a more quantitative understanding of this relationship we plotted the curvature values corresponding to the microseisms with the curvature values of the volume surrounding the hydraulic stimulation (Figure 5). This confirms that the events tend to occur in the small range of positive curvature values of 0.00006-0.00013.

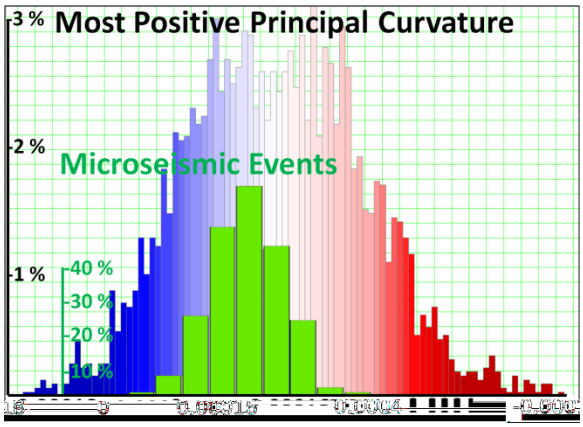

Figure 5. Most positive principal curvature range of microseismic occurrence for well A.

Acoustic Impedance Inversion

To further understand the behavior of the plotted microseisms, seismic inversion volumes were analyzed for several properties. Given that the seismic data was acquired prior to the hydraulic stimulation, the analysis of the acoustic impedance behavior aid in determining common factors that led to the subsequent known failure points.

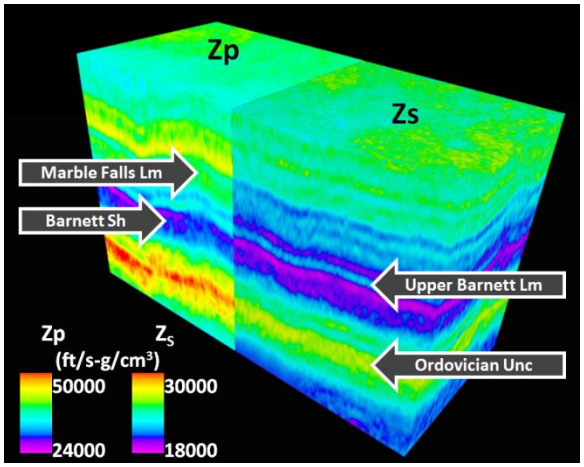

Figure 6. P-impedance and S-impedance volumes.

The model-based inverted volumes (e.g. Figure 6) were generated using pre-stack seismic, density and P and S-wave logs from five wells within the study area. The inversion method used was based on the three assumptions made by Hampson and Russell (2006), that the linearized approximation for reflectivity holds, that reflectivity as a function of angle can be given by the Aki-Richards equations, and that there is a linear relationship between the logarithm of P-impedance and both S-impedance and density.

By design, the microseisms occur primarily within the formation being stimulated, in this case the Lower Barnett Shale. Figure 7 shows how events targeted at the Lower Barnett Shale fall primarily within a narrow S-impedance range. Note several events leak into the Upper Barnett and even the Marble Falls. Impedance, and we hypothesize but have not yet demonstrated, mechanical properties, also vary within the formation. Locations of the microseismic events have a good correlation to the inversion volumes, where

they correspond to a narrow range of values for each property in all studied wells, regardless of their orientation and location.

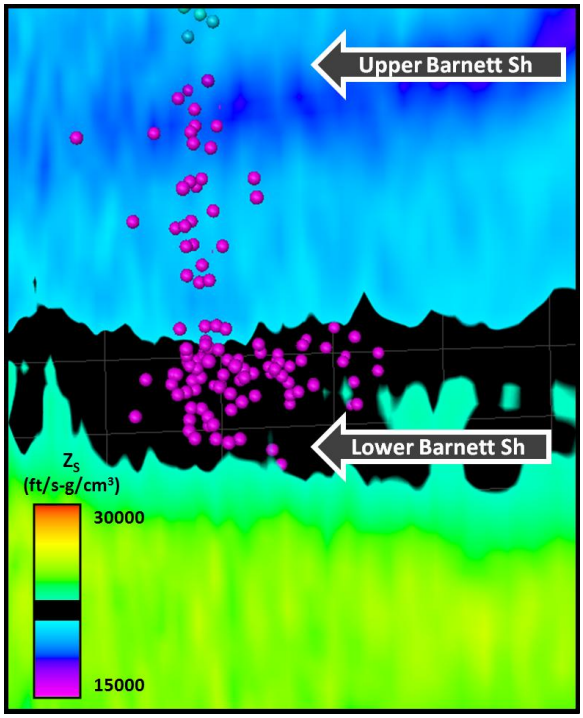

Figure 7. Microseisms within the Lower Barnett Shale S-impedance window (blacked out).

For a more quantitative approach, we plotted histograms of the impedance values corresponding to the microseisms with the impedance values found in the volume surrounding the stimulated area (Fig. 8). Events fall within a very similar P-impedance value of 31500-33500 ft/s*g/cm^3 (Fig 8a). Similarly, microseisms occur in S-impedance values of 19400-20100 ft/s*g/cm^3 (Fig 8b), where the formation appears more prone to fracturing. This predominant impedance range of microseismic occurrence is maintained throughout all stages and wells within our study area. Repeating this procedure for all the inverted properties shows similar results. The influence of the temporal patterns of microseismic activity on the property ranges where they occur is currently being studied.

Conclusions

Microseismic events associated with hydraulic fracturing are correlated to the regional stress patterns, curvature attributes, and the P- and S-impedance. Specifically, planes of weakness appear to be correlated to positive values of most positive volumetric curvature (anticlinal features) and P-impedance and S-impedance. Further calibration of this correlation should allow more accurately to predict possible fracture zones, lower risk, and stimulate more effectively a given target area.

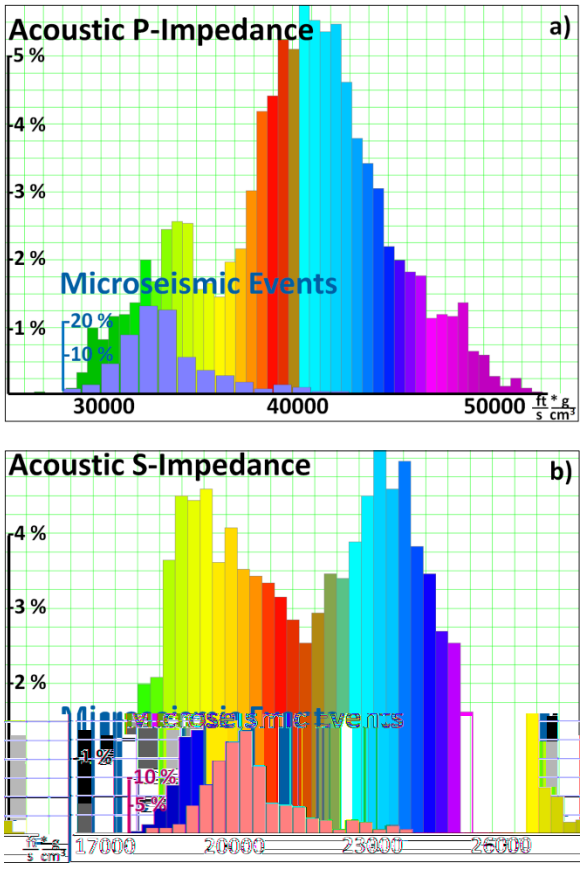

Figure 8 a) P-impedance range of microseismic occurrence for well A and b) S-impedance range of microseismic occurrence for well A.

Acknowledgments

We thank Devon Oil for providing financial support, data and permission to publish this work. Thanks to Schlumberger and Hampson-Russell for providing licenses used in interpretation and inversion process respectively.

EDITED REFERENCES

Note: This reference list is a copy-edited version of the reference list submitted by the author. Reference lists for the 2010 SEG Technical Program Expanded Abstracts have been copy edited so that references provided with the online metadata for each paper will achieve a high degree of linking to cited sources that appear on the Web.

REFERENCES

Abbott, D., S. Williams-Stroud, and R. Shaffer, 2009, Surface Microseismic Monitoring of Hydraulic Fracture Stimulations, Bakken Formation, Nesson Anticline, Williston Basin, North Dakota: Presented at the Annual Convention, AAPG.

Eisner, L., S. Williams-Stroud, A. Hill, P. Duncan, and M. Thornton, 2010, Beyond the dots in the box: Microseismicity-constrained fracture models for reservoir simulation: The Leading Edge, **29**, no. 3, 326, doi:10.1190/1.3353730.

Gale, J. F., R. M. Reed, S. P. Becker, and W. Ali, 2010, Natural fractures in the Barnett Shale in the Delaware Basin, Pecos Co. West Texas: comparison with the Barnett Shale in the Fort Worth Basin: Presented at the Annual Convention, AAPG.

Hampson, D. P., B. H. Russell, and B. Bankhead, 2006, Simultaneous Inversion of Pre-stack Seismic Data: Geohorizons, **11**, 13–17.

Mai, H. T., K. Marfurt, and S. Chávez-Pérez, 2009, Coherence and volumetric curvatures and their spatial relationship to faults and folds, an example from Chicontepec basin, Mexico: 79th Annual International Meeting, SEG, Expanded Abstracts, 1063-1067.

Neale C., 2010, Cost-effective, high-resolution hydraulic fracture microseismic monitoring – anywhere, anytime: E&P, 83, 46-48.

Williams-Stroud, S., and L. Eisner, 2009, Geological microseismic fracture mapping – methodologies for improved interpretations based on seismology and geologic context: 2009 Convention, CSPG CSEG SWLS, Expanded Abstracts, 501-504.

Williams-Stroud, S., and P. M. Duncan, 2008, Microseismic mapping –the geological factor: E&P, 81, 51-52.

Zhang, J., M. Bai, and J. C. Roegier, 2006, On drilling directions for optimizing horizontal well stability using a dual-porosity poroelastic approach: Journal of Petroleum Science Engineering, **53**, no. 1-2, 61–76, doi:10.1016/j.petrol.2006.02.001.